Gas Phase Hydration and Deprotonation of the Cyclic $C_3H_3^+$ Cation. Solvation by Acetonitrile, and Comparison with the Benzene Radical Cation

Ridha Mabrouki, Yehia Ibrahim, Enli Xie, Michael Meot-Ner (Mautner), and M. Samy El-Shall*

Department of Chemistry, Virginia Commonwealth University, Richmond, Virginia 23284-2006

Received: January 18, 2006; In Final Form: April 3, 2006

The binding energies of the first 5 H_2O molecules to *c*-$C_3H_3^+$ were determined by equilibrium measurements. The measured binding energies of the hydrated clusters of 9−12 kcal/mol are typical of carbon-based $CH^+\cdot\cdot\cdot X$ hydrogen bonds. The ion solvation with the more polar CH_3CN molecules results in stronger bonds consistent with the increased ion−dipole interaction. Ab initio calculations show that the lowest energy isomer of the *c*-$C_3H_3^+(H_2O)_4$ cluster consists of a cyclic water tetramer interacting with the *c*-$C_3H_3^+$ ion, which suggests the presence of orientational restraint of the water molecules consistent with the observed large entropy loss. The *c*-$C_3H_3^+$ ion is deprotonated by 3 or more H_2O molecules, driven energetically by the association of the solvent molecules to form strongly hydrogen bonded $(H_2O)_nH^+$ clusters. The kinetics of the associative proton transfer (APT) reaction $C_3H_3^+ + nH_2O \rightarrow (H_2O)_nH^+ + C_3H_2^\bullet$ exhibits an unusually steep negative temperature coefficient of $k = cT^{-63\pm4}$ (or activation energy of -37 ± 1 kcal mol^{-1}). The behavior of the $C_3H_3^+$/water system is exactly analogous to the benzene$^{+\bullet}$/water system, suggesting that the mechanism, kinetics and large negative temperature coefficients may be general to multibody APT reactions. These reactions can become fast at low temperatures, allowing ionized polycyclic aromatics to initiate ice formation in cold astrochemical environments.

I. Introduction

The chemistry of $C_3H_3^+$ has received considerable attention and continues to be an active area of research.[1−5] This is due to the important roles of the ion chemistry of $C_3H_3^+$ in flames and combustion processes particularly for the mechanisms of soot formation,[6,7] and in interstellar clouds particularly for the origin of larger hydrocarbon and other complicated molecular species observed in interstellar medium.[8−11] The $C_3H_3^+$ ions are also likely to be present in the hydrocarbon-containing ionospheres of Jovian planets,[12] Titan,[13] and in interstellar clouds.[8−11]

There are two low energy isomers of the $C_3H_3^+$ ion: the acyclic propargyl ion, H_2CCCH^+, and the cyclopropenyl ion, *c*-$C_3H_3^+$ which is more stable than the acyclic isomer by 24.9 kcal/mol.[14] The cyclic isomer *c*-$C_3H_3^+$ is, in fact, the smallest cyclic aromatic species. Correspondingly, *c*-$C_3H_3^+$ is stable and unreactive. For example, it is well-known that the reactivities of the H_2CCCH^+ ion with alkenes, alkynes, aromatic hydrocarbons, and alcohols are significantly higher than those of *c*-$C_3H_3^+$.[15,16]

The interactions of aromatic cations such as *c*-$C_3H_3^+$ with water and other polar solvent molecules are important in many chemical, astrochemical, physical and biological processes including, for example, solvation shells, hydrophobic hydration, clathrate formation, and proteins conformations.[17−19] Detailed information on these interactions can be provided by gas-phase studies where, for example, the binding energies of the solvent molecules in the inner shell of the hydrocarbon ions can be measured using gas-phase clustering equilibria.[20−22] Recently, we investigated the interactions of ionized aromatics with solvent molecules, including a detailed study of the benzene$^{+\bullet}$/water system, where we measured binding energies with up to eight water molecules bound to the benzene radical cation ($C_6H_6^{+\bullet}$).[20,21] In addition to building up clusters, the water molecules can also react with the core ions by extracting a proton.[20,21,23−26] Extraction of protons from ionized aromatics by solvent molecules may have important implications to reaction mechanisms, inhibition and termination of polymerization and to astrochemical processes.[25−29] For example, we observed recently the deprotonation of benzene$^{+\bullet}$ by several H_2O molecules, where the rate coefficients of the deprotonation reaction displayed an unprecedented large negative temperature coefficient of $k = cT^{-67\pm4}$ (or an activation energy of -34 ± 1 kcal/mol).[20,21] The deprotonation reaction is driven energetically by the formation of protonated water clusters, $(H_2O)_nH^+$, that contain a core hydronium ion (H_3O^+) and exhibit strong ionic hydrogen bonds (IHBs). Proton-transfer driven by the association of several molecules through exothermic bond formation may be called associative proton transfer (APT) reactions. These APT reactions can become very efficient under low-temperature astrochemical conditions where various polar molecules, which have proton affinities higher than H_2O, can co-condense on the hydrocarbon ions and further facilitate the deprotonation of the ions.

In this paper we shall study the solvation of *c*-$C_3H_3^+$ ions and their deprotonation by water through APT reactions. In comparison with the benzene radical cation $C_6H_6^{+\bullet}$, the *c*-$C_3H_3^+$ ions present two interesting features. First, the size of the ion is significantly smaller than that of $C_6H_6^{+\bullet}$ and, therefore, the charge density on *c*-$C_3H_3^+$ is significantly higher than in $C_6H_6^{+\bullet}$. Second, the proton affinity of the $C_3H_2^\bullet$ radical (227 kcal/mol) is significantly higher than that of the phenyl radical $C_6H_5^\bullet$ (212 kcal/mol).[30] These features could provide valuable insights on

* Corresponding author. E-mail: selshall@hsc.vcu.edu.

10.1021/jp0603684 CCC: $33.50
Published on Web 05/20/2006

the important factors that control binding energies, structures and the extent of the deprotonation reactions by comparing the $C_6H_6^{+\bullet}$/water and the *c*-$C_3H_3^+$/water systems.

In the present study, we also provide a comparison of the solvation of $C_6H_6^{+\bullet}$ and the *c*-$C_3H_3^+$ with acetonitrile molecules. Unlike water molecules where an extended hydrogen bonding network may facilitate the transfer of the proton from the hydrocarbon ion, acetonitrile molecules cannot form hydrogen bonding networks because of the presence of the blocking CH_3 terminal groups.[31,32] In this case, the comparison between water and acetonitrile could shed more light on the structural factors that influence the extent of deprotonation via APT reactions. The aim of this work is to establish a unified molecular level understanding of the roles of hydrogen bonding and dipole−dipole interactions in determining the structures of the solvated hydrocarbon ions and the mechanism of the overall deprotonation reactions.

II. Experimental and Computational Methods

The experiments were performed using the VCU mass-selected ion mobility spectrometer. The details of the instrument can be found in several publications and only a brief description of the experimental procedure is given here.[33−35]

Mass-selected $C_3H_3^+$ ions (*m*/*z* 39, generated by electron impact ionization of benzene vapor) are injected (in 5−15 μs pulses) into the drift cell (the inner diameter and length of the total cell are 8.1 and 8.9 cm, respectively.) containing 2 Torr of He for the mobility measurements or 0.2−0.4 Torr of pure H_2O or CH_3CN vapor (Aldrich, HPLC grade) for the equilibrium measurements. Flow controllers (MKS # 1479A) are used to maintain a constant pressure inside the drift cell. The temperature of the drift cell can be controlled to better than ±1 K using six temperature controllers. Liquid nitrogen flowing through solenoid valves is used to cool the drift cell and cartridge heaters are used to heat the cell. The reaction products are identified by scanning a second quadrupole mass filter located coaxially after the drift cell. The arrival time distributions (ATD) are collected by monitoring the intensity of each ion as a function of time. The reaction time can be varied by varying the drift voltage. The injection energies used in the experiments (5−20 eV, laboratory frame) are slightly above the minimum energies required to introduce the ions into the cell against the H_2O flow. Most of the ion thermalization occurs outside the cell entrance by collisions with the water vapor escaping from the cell entrance orifice.[33−35]

At a cell pressure of 0.2 Torr, the number of collisions that the $C_3H_3^+$ encounters from the water molecules within the 1.5 ms residence time inside the cell is about 10^4 collisions, which is sufficient to ensure efficient thermalization of the $C_3H_3^+$ ions.

The ATDs of the injected $C_3H_3^+$ and the $C_3H_3^+(H_2O)_n$ formed inside the cell are measured as a function of the drift voltage across the cell. The intensity ratio of ions in the association equilibrium, $I[(C_3H_3^+)(H_2O)_n]/I[(C_3H_3^+)(H_2O)_{n-1}]$ is measured from the integrated peak areas of the ATDs at the known temperatures and pressures. The equilibrium constants are then obtained using

$$K_{eq} = I[C_3H_3{}^+(H_2O)_n]/I[C_3H_3{}^+(H_2O)_{n-1}]P(H_2O) \quad (1)$$

Here *I* is the intensity of the peaks taken from the ATDs and $P(H_2O)$ is the partial pressure of the water vapor inside the drift cell. All the equilibrium experiments are conducted at low drift cell fields of 1 V/cm and corresponding long residence times of 3 ms. The equilibrium constants measured as a function of temperature yield $\Delta H°$ and $\Delta S°$ from the slopes and intercepts, respectively of the van't Hoff plots. All of the results are replicated three or more times.

To further test the equilibrium, the residence times of the ions are varied by applying drift fields of 1−4 V/cm inside the drift cell at 302 K and $P(H_2O) = 0.3$ Torr. Under these conditions the ion residence times vary between 0.4 and 3.0 ms. The observed equilibrium constants are independent of reaction time, which further demonstrates that equilibrium is established during the observable reaction times.

The structures of the ions are optimized at the ROHF/6-31+G(d,p), B3LYP/6-31+G** and MP2/6-31+G** levels of theory using the Gaussian G03 software package.[36] The optimization is verified by calculating the vibrational frequencies. The cluster binding energies are corrected for the zero-point energies and the basis-set superposition error (BSSE). The BSSE is calculated using the Counterpoise method as implemented in the G03 software. The charge on each component within each cluster is calculated by adding all atomic Mulliken charges.

III. Results and Discussion

1. Mobility and Structure of the $C_3H_3^+$ Ion. The $C_3H_3^+$ ions are generated in our experiments by EI fragmentation of benzene vapor. It is generally assumed that the fragment $C_3H_3^+$ ion is the cyclopropenyl cation (*c*-$C_3H_3^+$) and that the neutral radical fragment has the linear CH_2CCH structure.[37−39] However, in our experiments mobility measurements are performed to confirm the structure of the injected $C_3H_3^+$ ions. For these experiments, He (ultrahigh purity, Spectra Gases 99.999%) is used as the buffer gas. The mobility *K* of an ion is defined as[40]

$$K = \vec{v}_d/\vec{E} \quad (2)$$

where $\vec{v}_d$ is the drift velocity and $\vec{E}$ is the field across the drift region. The reduced mobility K_0 (scaled to the number density at standard temperature and pressure STP) is given by

$$K_0 = \frac{273.15P}{760T} K \quad (3)$$

where *P* is the pressure in Torr and *T* is the temperature in Kelvin. Equations 2 and 3 can be combined and rearranged to give

$$t_d = \left(\frac{273.15l^2}{760T}\frac{1}{K_0}\right)\frac{P}{V} + t_0 \quad (4)$$

where *l* is the drift length, t_d is the measured mean arrival time of the drifting ion packet taken from the center of the ATD peak, t_0 is the time the ion spends outside the drift cell before reaching the detector, and *V* is the voltage across the drift cell. Mobility is determined according to eq 4, by plotting t_d versus *P*/*V*. The slope of the linear plot is inversely proportional to the reduced mobility and the intercept equals the time spent within the second quadrupole before the detection of the ions.

Figure 1 displays the mass spectrum of the mass-selected $C_3H_3^+$ ions injected in pure helium, and the inset figure illustrates the variation of the ATDs with P/V used to calculate the mobility of $C_3H_3^+$. The reduced ion mobility is related to the average collision cross section of the ion with the buffer gas according to eq 5 of the kinetic theory:[41]

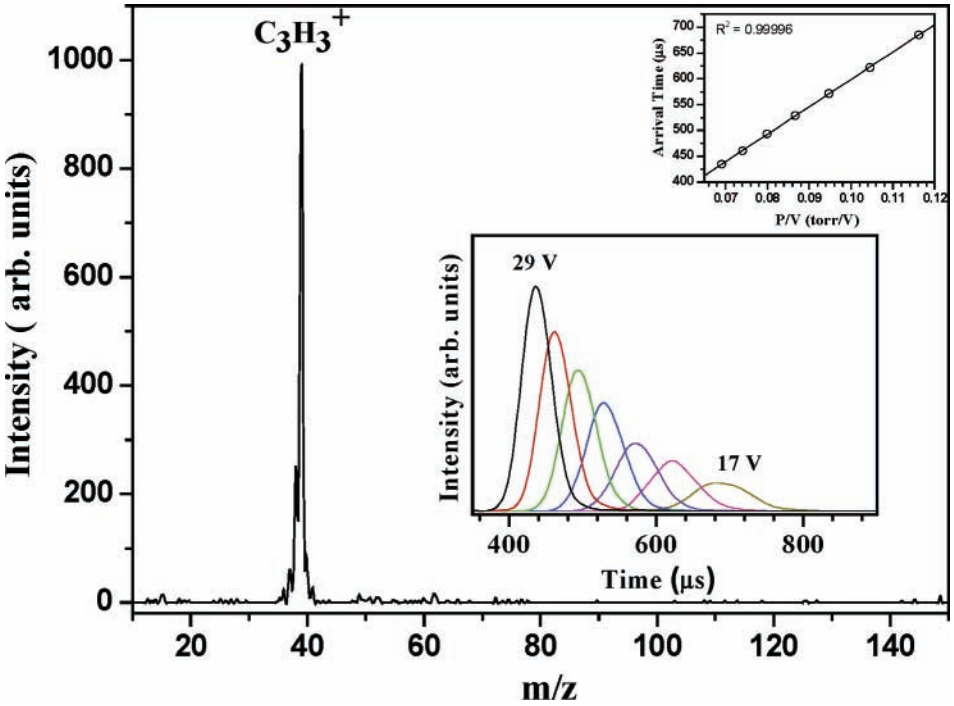

Figure 1. Mass spectrum obtained following the injection of $C_3H_3^+$ into the drift cell containing pure helium at 2.5 Torr and temperature of 273 K. The large inset displays the arrival time distributions (ATDs) of the $C_3H_3^+$ ion at different drift voltages (decreasing from left to right). The small inset shows a plot of mean arrival time (t_0) of $C_3H_3^+$as a function of P/V (Torr V^{-1}).

$$K = \frac{1}{N}\frac{(18\pi)^{1/2}}{16}\left[\frac{1}{m}+\frac{1}{m_b}\right]^{1/2}\frac{ze}{(k_BT)^{1/2}\Omega^{(1,1)}_{avg}} \qquad (5)$$

where N is the buffer gas number density, m is the mass of the ion, m_b is the mass of a buffer gas atom, z is the number of charges, e is the electron charge, k_B is Boltzmann's constant and $\Omega^{(1,1)}_{avg}$ is the average collision integral. The optimized geometry of the cyclic *c*-$C_3H_3^+$ ion was obtained at the MP2/6-31+G** level of theory, and for the propargyl isomer we used the structure reported in ref 42. These structures (shown in Figure 2) are used to obtain average collision cross-sections using the trajectory calculations which employ a potential consisting of LJ and ion-induced dipole interactions.[43] At 303 K, the measured cross-section of the C_3H_3 ions in He is 32.9 Å^2, somewhat closer to the calculated Ω of 34.5 Å^2 for the cyclic isomer than to Ω of 36.6 Å^2 calculated for the propargyl structure. This and the observation of only one ATD peak in our experiments at lower temperatures under high-resolution mobility conditions, confirm that the $C_3H_3^+$ ion generated in our experiments has the cyclic structure.

To further confirm the structure of the injected $C_3H_3^+$ ion, ~0.05 Torr of C_2H_4 and 0.3 Torr of pure water vapor are introduced into the drift cell, similar to the conditions used for the equilibrium measurements below. If linear $C_3H_3^+$ is present, it will react with C_2H_4 with a half-life of about 4×10^{-7} s under our conditions, much faster than the millisecond range drift time; i.e., all of the linear isomer will be converted to form the $C_5H_5^+$ (*m*/*z* 65) ion, whereas the cyclic isomer is unreactive.[44] The mass spectrum does not show the appearance of new products under these conditions and the equilibrium distribution of the clusters is also not affected by the presence of ethylene. Therefore, both the mobility and reactivity tests confirm that the observed ion is the *c*-$C_3H_3^+$ isomer. If the EI ionization of benzene produces both linear and cyclic isomers in our experiments, then we must assume that the linear ions ($\Delta H°_f$-($HCCCH_2^+$) = 282 kcal/mol) rearrange to the more stable cyclic isomers ($\Delta H°_f$(*c*-$C_3H_3^+$) = 257 kcal/mol) during the injection

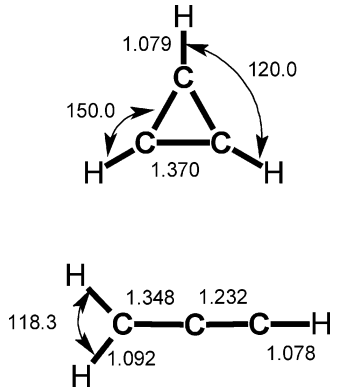

Figure 2. Ab initio structures of the cyclopropenyl ion (*c*-$C_3H_3^+$) obtained at the MP2/6-31+G** level (this work), and the linear propargyl ion (H_2CCCH^+) (ref 42).

of the ions into the drift cell where the injection energy is higher than the barrier to isomerization of the $HCCCH_2^+$ ions.[38,39] This isomerization is also assisted by association with water molecules in the drift cell. In fact, theoretical calculations showed that the isomerization barrier from the linear propargyl ion to *c*-$C_3H_3^+$ vanishes with three water molecules associated with the propargyl ion.[42]

2. Thermochemistry of Hydration of the *c*-$C_3H_3^+$ Ion. Figure 3 displays the mass spectra of the $C_3H_3^+/H_2O$ system obtained at different temperatures. The mass spectra show the $C_3H_3^+W_n$ clusters (W = H_2O) and the protonated water clusters (W_nH^+) formed by the deprotonation of the $C_3H_3^+$ ions. At 60 °C, the cluster population shows the $C_3H_3^+W_n$ sequence with n = 1 and 2, and the W_nH^+ series starting from n = 4. As the temperature decreases, the ion intensity of $C_3H_3^+$ decreases and the $C_3H_3^+W_n$ sequence increases with the highest value of n = 6 clearly observed at 18 °C. The population of the W_nH^+ series also shifts to higher n with decreasing temperature. However, we note that in the bottom panel of Figure 3 the $C_3H_3^+W_n$ cluster populations decrease at n = 3 and increase again with a

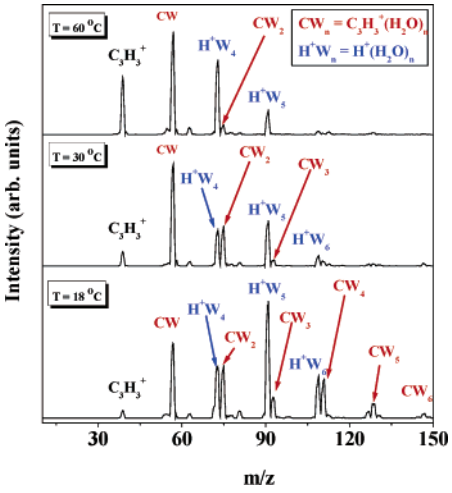

Figure 3. Mass spectra obtained following the injection of $C_3H_3^+$ ions (*m*/*z* 39) into 0.30 Torr of pure H_2O vapor at different temperatures.

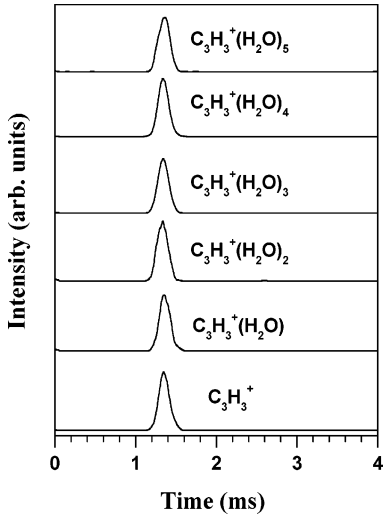

Figure 4. Arrival time distributions (ATDs) of $C_3H_3^+(H_2O)_n$ clusters, $n = 0-5$, obtained by injecting $C_3H_3^+$ ions (*m*/*z* 39) into 0.28 Torr of pure at H_2O vapor at 18 °C.

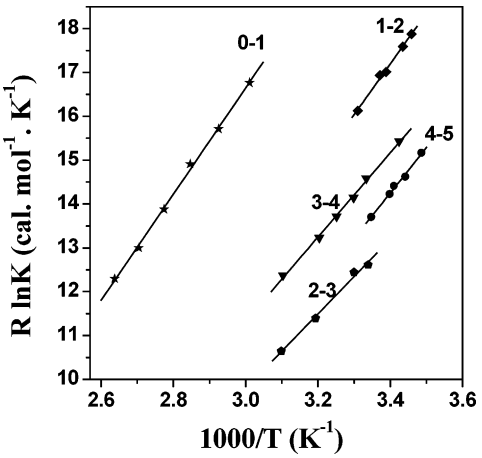

Figure 5. van't Hoff plots for the clustering equilibria: $C_3H_3^+(H_2O)_{n-1} + H_2O \rightarrow C_3H_3^+(H_2O)_n$ represented by $(n-1)-n$, with $n = 1-5$.

maximum at $n = 4$. The higher clusters, $C_3H_3^+W_n$, with $n > 4$ remain the smallest cluster peaks under any observed conditions.

In the $C_3H_3^+/H_2O$ system the overall APT reaction is given by

$$C_3H_3^+ + nH_2O \rightarrow (H_2O)_nH^+ + C_3H_2^{\bullet} \qquad (6)$$

However, we observe in Figure 3 an equilibrium population of stabilized hydrated clusters $C_3H_3^+(H_2O)_n$, and the APT can proceed from these clusters as in reaction 7.

$$C_3H_3^+(H_2O)_{n-1} + H_2O \rightarrow (H_2O)_nH^+ + C_3H_2^{\bullet} \qquad (7)$$

Both reactions 6 and 7 are endothermic for small *n* but become exothermic at sufficiently large *n* because of the stability of the product protonated water clusters. In fact, the energetics of the reaction show that reaction 7 turns from endothermic into approximately thermoneutral at $n = 4$ corresponding to the $C_3H_3^+(H_2O)_3$ reactant. The weak minimum at $C_3H_3^+(H_2O)_3$ in the cluster distribution at 18 °C shown in Figure 3, may suggest that the side reaction competes with the equilibrium processes, thus resulting in depletion of the ion intensity of the $C_3H_3^+$-$(H_2O)_3$ cluster. We observed a similar distribution in the benzene$^{+\bullet}$/water system but with a more pronounced minimum at the benzene$^{+\bullet}(H_2O)_3$ cluster. In that system, the competition from the deprotonation reaction was strong enough to prevent the establishment of equilibrium between the benzene$^{+\bullet}(H_2O)_3$ and benzene$^{+\bullet}(H_2O)_3$ species.[20,21] However, in the present $C_3H_3^+$/water system, this effect appears to be negligible because no shift in the ATDs is observed and the equilibrium appears to be established among the observed $C_3H_3^+(H_2O)_n$ ions. A good test of equilibrium comes from the identical ATDs of the ions coupled by equilibrium. If the $C_3H_3^+$ and $C_3H_3^+(H_2O)_n$ ions are in equilibrium, their ATDs must be identical. This is evident from the ATDs shown in Figure 4 for the $C_3H_3^+(H_2O)_n$ ions with $n = 0-5$. The equilibrium constants for the stepwise hydration of $C_3H_3^+$ (eq 1) yield the van't Hoff plots shown in Figure 5. The resulting $\Delta H°$ and $\Delta S°$ values are listed in Table 1.

The measured thermochemical values shown in Table 1 are unusual in that the binding energies of $C_3H_3^+(H_2O)_n$ do not follow the usual regular decrease with *n* observed in typical ion solvation.[22] This could suggest that there are several binding sites with comparable energies for the water molecules to attach to the $C_3H_3^+$ ion. The *c*-$C_3H_3^+$ ion has three equivalent hydrogens that can form $CH^{\delta+}\cdots OH_2$ hydrogen bonds, and the observed values are consistent with the usual strengths of such bonds of about 10 kcal/mol.[22,45-47] The bonds in this system are stronger by a few kcal/mol than in the respective clusters of $C_6H_6^{+\bullet}$ because of the higher charge density on the $C_3H_3^+$ ion as compared to $C_6H_6^{+\bullet}$. However, these bond strengths are also similar to the 8−10 kcal/mol bonds of $OH^{\delta+}\cdots OH_2$ bonds in large hydrated clusters.[22] Therefore, the $C_3H_3^+(H_2O)_n$ ($n = 2$ and 3) clusters may have isomers of comparable energies with direct bonds to the core ion (internal solvation) and with the outer shell water−water bonds (external solvation). The structures of the low energy isomers obtained from ab initio calculations will be discussed in the next section. These isomers

TABLE 1: Thermochemistry[a] of the Hydration Equilibria $C_3H_3^+(H_2O)_{n-1} + H_2O = C_3H_3^+(H_2O)_n$

n	$\Delta H°$ (kcal·mol^{-1})	$\Delta S°$ (cal·mol^{-1}·K^{-1})
1	−11.7	−18.8
2	−10.3	−17.2
3	−8.5	−15.8
4	−12.0.3	−25.0
5	−10.0	−19.6

[a] Error estimate for experimental values from standard deviations of van't Hoff and from usual uncertainties in clustering equilibrium temperature studies: $\Delta H° \pm 1$ kcal/mol, $\Delta S° \pm 3$ cal·mol^{-1}·K^{-1}.

may be in equilibrium in the observed populations, as observed in other cluster systems.[22,48]

Because the *c*-$C_3H_3^+$ ion has three equivalent hydrogens that can form $CH^{\delta+}\cdots OH_2$ hydrogen bonds, it may appear that the fourth H_2O molecule about $C_3H_3^+$ must necessarily be in an outer shell. Formation of a new shell can lead to a drop in the binding energies,[22,47] but in the present case the binding energies of the weak $CH^{\delta+}\cdots OH_2$ bonds have similar energies to the usual $OH^+\cdots OH_2$ bonds in outer shells, and in such cases forming a new shell does not lead to a drop in the binding energies.[22,47] In fact, the measured bonding energy of *c*-$C_3H_3^+(H_2O)_n$ increases rather than decreases at $n = 4$, and this may suggest the formation of a cyclic water tetramer within the *c*-$C_3H_3^+(H_2O)_4$ cluster, which could provide stronger binding as compared to a solvation shell consisting of three water molecules with the fourth molecule in an outer shell. In fact, the calculated structures discussed below provide evidence for this speculation. Another experimental result consistent with the formation of a cyclic water tetramer is the sudden increase in the $-\Delta S^\circ_{3,4}$ value, which suggests the presence of orientational restraint of the water molecules as a result of the connectivity between the four water molecules in a ring-like structure.[49] This point will be further discussed with the calculated structures of the $C_3H_3^+(H_2O)_4$ isomers. As noted above, at this cluster size the measured values may also reflect effects of the deprotonation side-reaction, although the equal ATDs in Figure 4 suggest that we observe the equilibrium in all steps.

3. Structures and Binding Energies of the Hydrated *c*-$C_3H_3^+$ Ions. Figure 6 displays the calculated structures for some low energy isomers obtained from the ab initio calculations at the MP2/6-31+G** level along with their energies relative to the most stable isomer of each cluster. The structures of the lowest energy isomers of *c*-$C_3H_3^+(H_2O)_n$ with $n = 0-4$ are shown in Figure 7.

Two isomers were obtained for the *c*-$C_3H_3^+(H_2O)$, as shown in Figure 6A; isomer 1-a is more stable than isomer 1-b by 0.7 kcal/mol due to the aligned hydrogen bond between the water oxygen atom and the $C_3H_3^+$ hydrogen atom. The charges on *c*-$C_3H_3^+$ are equally distributed and localized among the carbon atoms (90% of the charge). Upon clustering with one water molecule, the charge distribution changes with significant localizations on the hydrogen atoms of the *c*-$C_3H_3^+$, and one C−H bond shows elongation resulting from the linear H-bond formation with the oxygen atom of the water molecule. Clustering of the second water molecule starting from isomer 1-a gives the most stable internally solvated $C_3H_3^+(H_2O)_2$ ion (isomer 2-a in Figure 6B). The bond lengths and charge distributions are very symmetric on isomer 2-a. The other three higher energy isomers (2-b, 2-c and 2-d) all involve water−water interactions with isomer 2-c (1 kcal/mol higher in energy than the most stable isomer 2-a) showing the shortest H-bonds between water and *c*-$C_3H_3^+$ ($H_2O\cdots HC_3H_2^+$, 1.748 Å) and between water−water ($H_2O\cdots HHO.HC_3H_2^+$, 1.792 Å).

On the basis of the structure of the $C_3H_3^+$ ion, the $C_3H_3^+(H_2O)_3$ cluster is expected to mark the first solvation shell around the $C_3H_3^+$ ion. However, the solvated ion structure (3-d) is higher in energy by 2 kcal/mol than the most stable isomer (3-a), as shown in Figure 6-C. interestingly, the lowest energy isomer (3-a) shows the three water molecules forming a cyclic trimer that interacts with the $C_3H_3^+$ ion. This structure is clearly very different from the classical ion solvation structure that involves H-bonds with the hydrogens of the *c*-$C_3H_3^+$ ion. This indicates that the water−water hydrogen bonding interaction within the cyclic water trimer can provide more stability to the $C_3H_3^+(H_2O)_3$ cluster than that provided by the solvated ion structure (3-d) where the three water molecules participate as acceptors to the hydrogens of the $C_3H_3^+$ ion. The second lowest energy isomer (3-b), 1.2 kcal/mol higher in energy than 3-a, indicates that the water−water interaction, although not in a cyclic structure, can still provide extra stability over the solvation shell structure (3-d). The third isomer (3-c) represents a structure that involves both the ion solvation and hydrogen bonding interactions among the three water molecules. This isomer (3-c) has energy similar to that of the solvated ion isomer (3-d) that involves no hydrogen bonding interaction between the water molecules.

The addition of the fourth water molecule produces structure 4-a as the lowest energy isomer of the $C_3H_3^+(H_2O)_4$ cluster. The known water tetramer cyclic structure[49,50] binds with two long hydrogen bonds to the $C_3H_3^+$ hydrogens and provides the lowest energy isomer (4-a). The second isomer (4-b), 2.2 kcal/mol higher in energy than isomer 4-a, has the fourth water molecule hydrogen bonded to the cyclic water trimer which is located above the $C_3H_3^+$ ion. The third lowest energy isomer (4-c) is higher in energy by 5 kcal/mol than isomer 4-a and has a very different structure in which the fourth water molecule starts to form a second solvation shell through hydrogen bonding to water in the first solvent shell. This isomer (4-c) and all other isomers are higher in energies by 5−9 kcal/mol relative to isomer 4-a. It is quite interesting that the lowest energy isomers of the $C_3H_3^+(H_2O)_3$ and the $C_3H_3^+(H_2O)_4$ clusters involve the formation of a cyclic water trimer and tetramer, respectively. This propensity of water molecules to form cyclic structures in the presence of the *c*-$C_3H_3^+$ ion is consistent with the structural behavior of neutral water clusters.[49,50]

The calculated binding energies at three different levels of theory after the BSSE corrections for the $C_3H_3^+(H_2O)_n$ clusters with $n = 1-3$ agree reasonably well with the experimental values, as shown in Table 2. However, it is clear that the interatomic distance between the O atom of water and the H atom of the $C_3H_3^+$ ion in the $C_3H_3^+(H_2O)$ cluster is highly sensitive to the degree of electronic correlations as shown Table 2. The lowest energy structures presented in Figures 6 and 7, obtained with full geometry optimizations at the MP2/6-31+G** level, are expected to capture most of the electronic correlation effects. The BSSEs are calculated in cases where the addition of a water molecule to the lowest energy isomer of the $(n - 1)$ cluster results, after geometry optimization, in the lowest energy isomer of the (n) cluster. For the $C_3H_3^+(H_2O)_4$ cluster the addition of the fourth water molecule to the lowest energy isomer (3-a) does not produce the lowest energy isomer of the $C_3H_3^+(H_2O)_4$ cluster (4-a). Therefore, the binding energy calculated on the basis of the lowest energy isomer of the $C_3H_3^+(H_2O)_4$ cluster (11.99 kcal/mol at the MP2/6-31+G** level in comparison with the experimental value of 12.3 kcal/mol) does not include the BSSE correction. It should be noted that the presence of several isomers with comparable energies and many different connecting pathways make the calculations of the BSSEs and, therefore, the corrected binding energies, uncertain for the large clusters. It should be clear, however, that the experimental binding energy in these systems may reflect an average of several possible structural isomers with comparable energies.

4. Kinetics and Energetics of the Deprotonation Reactions. The APT reaction (2) or (3) converts the populations of the equilibrium-coupled $C_3H_3^+(H_2O)_n$ clusters to populations of protonated water clusters $(H_2O)_nH^+$. Figure 8a (left) illustrates the change of ion concentration−time profiles due to this

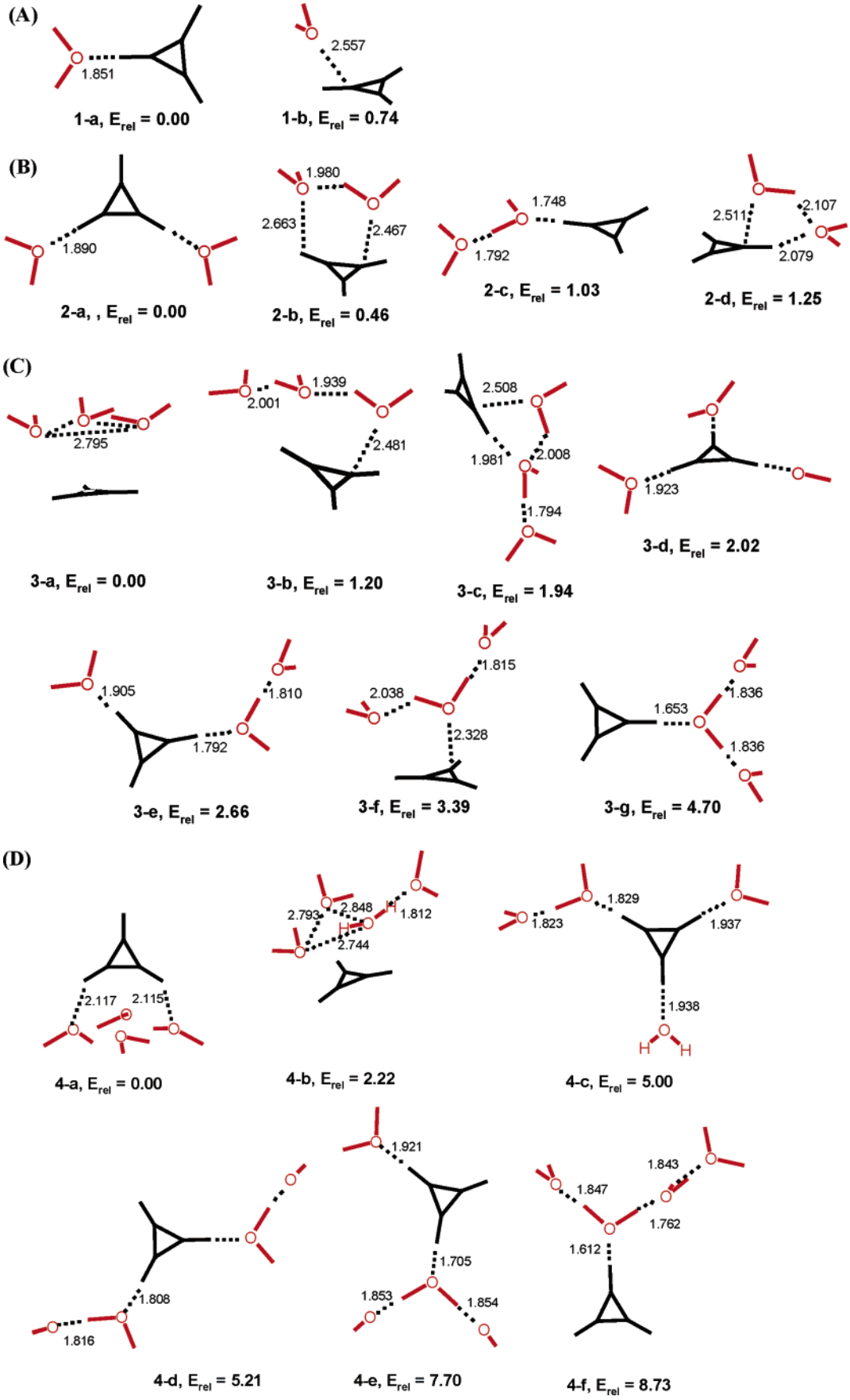

Figure 6. (A, B) Structures of c-$C_3H_3^+(H_2O)_n$ isomers for $n = 1$ and 2 calculated at the MP2/6-31+G** level. (C) Structures of c-$C_3H_3^+(H_2O)_3$ isomers calculated at the MP2/6-31+G** level. (D) Structures of c-$C_3H_3^+(H_2O)_4$ isomers calculated at the MP2/6-31+G** level. E_{rel} is the energy (kcal·mol^{-1}) relative to the most stable isomer for each n. Bond lengths are in angstroms.

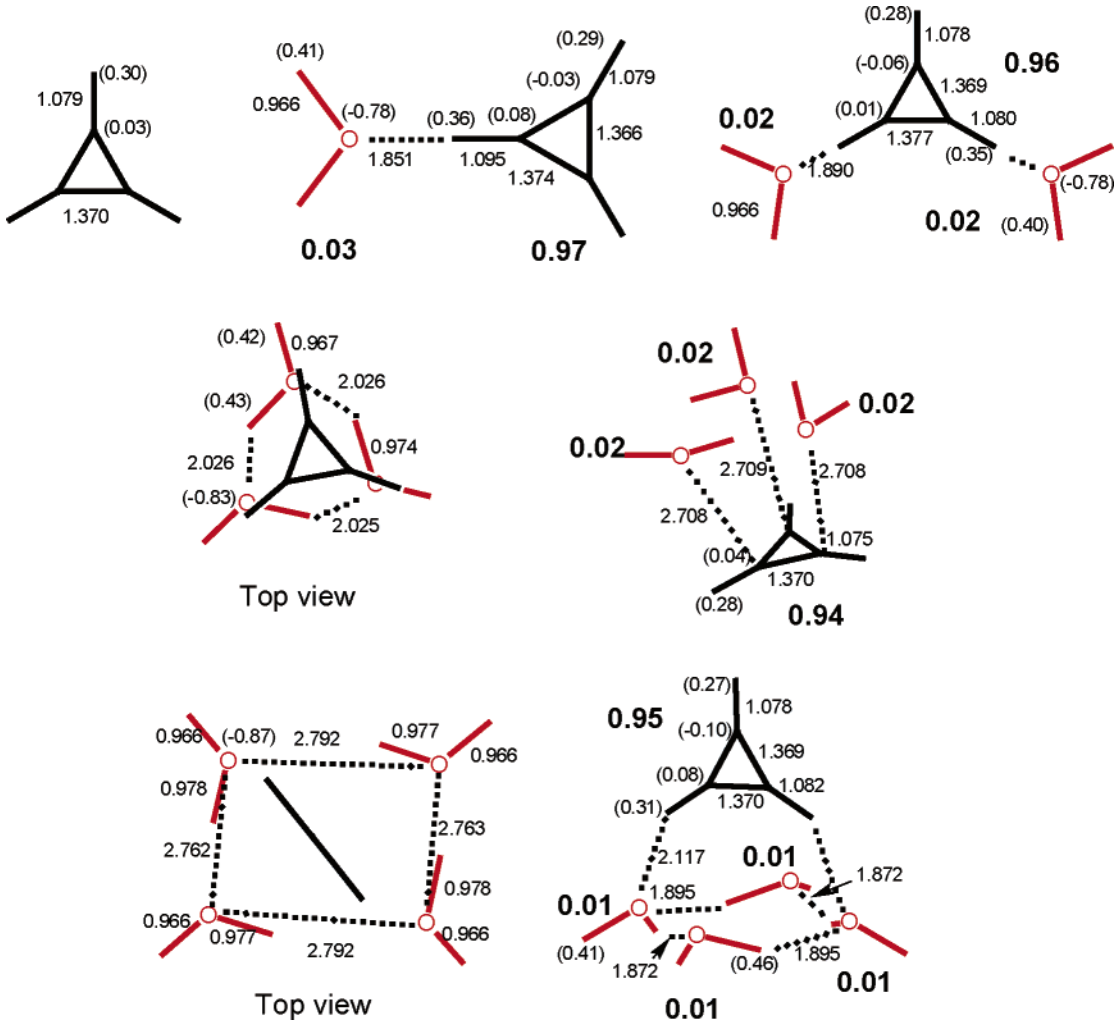

Figure 7. Lowest energy isomers of c-$C_3H_3^+$ and c-$C_3H_3^+(H_2O)_n$ clusters calculated at the MP2/6-31+G** level. Bond lengths are in angstroms, the atomic charges are in parentheses and molecular charges (sum of all atomic charges) are in bold.

TABLE 2: Binding Energies (kcal/mol) of the $C_3H_3^+(H_2O)_n$ Clusters Calculated at Different Levels of Theory[a]

n	MP2//ROHF/ 6-31+G**[b]	B3LYP/ 6-31+G**[c]	MP2/ 6-31+G**[d]	exp
1	11.95 (13.71)	12.70 (13.60)	11.83 (13.78)	11.7
2	10.74 (12.47)	10.91 (11.81)	10.51 (12.46)	10.3
3	9.67 (11.41)	9.21 (10.14)	(10.61)	8.5
4	(10.20)	(9.05)	(11.99)	12.3
CH...OH_2 (Å)	1.946	1.806	1.851	

[a] The values between brackets do not include BSSE; only ZPVE is included. [b] MP2 energies on the optimized ROHF/6-31+G(d,p) structures. [c] Optimized at the B3LYP/6-31+G** level. [d] Optimized at the MP2/6-31+G** level.

reaction. We can calculate the pseudo-first-order rate coefficients from the decay of the normalized intensities of the $C_3H_3^+(H_2O)_n$ clusters using plots of $\ln(\Sigma I[C_3H_3^+(H_2O)_n]/(\Sigma I[C_3H_3^+(H_2O)_n] + \Sigma I[(H_2O)_nH^+]))$ vs t (drift time) of the $C_3H_3^+(H_2O)_n$ clusters, where the sums are over the intensities of the ATD peaks of all the observable clusters at any given temperature. As in the benzene$^{+\bullet}$/water system, the rate coefficients show very large negative temperature coefficients, which may be obtained from the plot of ln k vs ln T in the exponential form as $k = cT^{-63\pm4}$ or as an Arrhenius activation energy of -37 ± 1 kcal/mol as shown in Figure 8 (right) (error estimates based on standard deviations of the slopes of the plots).

Negative temperature coefficients were observed in bimolecular ion−molecule reactions in hindered reactants, and

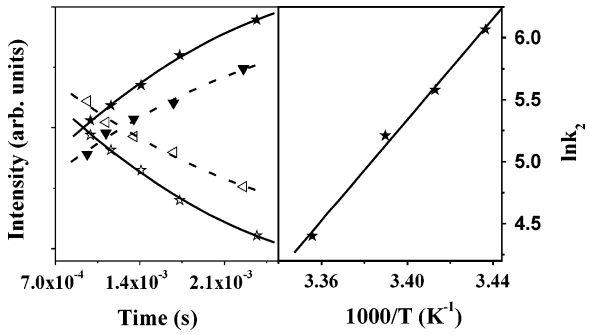

Figure 8. (left) Concentration−time profiles of the sums of the $C_3H_3^+(H_2O)_n$ ions (full triangles and full stars) and of the product $(H_2O)_nH^+$ ions (open triangles and open stars) as a function of reaction time as measured by the drift time of the $C_3H_3^+(H_2O)_n$ ions in the mobility cell in neat water vapor at $P(H_2O) = 0.24$ Torr. Solid lines: $T = 279$ K. Dotted lines: $T = 293$ K. (right) Plot of ln k vs 1000/T (K^{-1}).

in association reactions.The observed temperature coefficients of $k = cT^{-2}$ to cT^{-8} are due to competitive dissociation of the reaction complexes to products or back to reactants.[48] However, the much larger temperature coefficients of the deprotonation reactions in $C_3H_3^+$/water, and in benzene$^{+\bullet}$/water systems, may be attributed to a different source. In these cases a many-body cluster $C_3H_3^+(H_2O)_n$ ($n = 3$) needs to be assembled first to make the deprotonation reaction 7 energetically possible. These clusters may be seen as the reactive fraction of the overall cluster populations. This reactive fraction of the equilibrium cluster

populations increases with decreasing temperature. The cumulative enthalpy change for forming the $C_3H_3^+(H_2O)_n$ clusters is the sum of the association enthalpies of the first n steps, respectively. In the present system this enthalpy change is −30.5 kcal/mol for $n = 3$ and −43.0 kcal/mol for $n = 4$, in same range as the observed Arrhenius activation energy of −37 kcal/mol. We found a similar relation between thermochemistry and kinetics in the benzene$^{+\bullet}$/water system.[20,21]

As to the energetics of the deprotonation reactions, we may consider the energetics of the overall reaction 6 or of the stepwise reaction 7 above. The energetics may be calculated from the proton affinities of H_2O (165 kcal/mol) and of the *c*-$C_3H_2^\bullet$ radical (227 kcal/mol),[30] the binding energies of the $(H_2O)_nH^+$ clusters of 32, 21, 18, and 13 kcal/mol for $n = 2-5$, respectively,[51] and, for reaction 7, the binding energies of the $C_3H_3^+(H_2O)_n$ clusters (Table 2). For the overall reaction 6 we find, for deprotonation by n H_2O molecules, ($n = 1$ to 5) the $\Delta H°$ values of 62, 30, 10, −7 and −20 kcal/mol. Therefore, the overall reaction becomes exothermic for deprotonation by 4 H_2O molecules. For the stepwise reaction 7, deprotonation by a total of 1−5 H_2O (i.e., with *n* going from 1 to 5 in reaction 7) has $\Delta H°$ values of 62, 41.7, 20.3, 1.5 and −7.7 kcal/mol, respectively. Thus, this reaction becomes about thermoneutral at the deprotonation of the 3-fold solvated ion $C_3H_3^+(H_2O)_3$, and exothermic at the deprotonation of the 4-fold solvated ion $C_3H_3^+(H_2O)_4$.

The thermochemistry of the overall reaction 6 is relevant if the reaction proceeds effectively in one step, i.e., if the cluster is assembled without stabilization, retaining the exothermicity of all the association steps as internal energy for deprotonation/dissociation to form products. This may be possible in the experiments that use neat water vapor, where collision with every successive H_2O molecule can lead to association with the release of the binding energy into internal energy, rather than removing energy from the cluster. However, if a third body is present, it would stabilize the growing cluster and no internal energy would be available for deprotonation/dissociation. In fact, we observed such a third-body effect in the benzene$^{+\bullet}$/water system where the addition of He quenched the deprotonation reaction.[21]

The stepwise reaction 7 becomes near thermoneutral with deprotonation of the 3-fold solvated cluster by the fourth H_2O molecule, which is consistent with the observed results. An intermediate mechanism, where the incipient clusters are partially thermalized between steps is also possible. Clearly, the mechanism of associative transfer reactions requires further studies.

5. Solvation of $C_6H_6^{+\bullet}$ and *c*-$C_3H_3^+$ by Acetonitrile. Given the similar behaviors of the $C_6H_6^{+\bullet}$ and *c*-$C_3H_3^+$ ions with respect to the hydration and deprotonation reactions, it is interesting to examine the solvation of these ions with a nonprotic solvent molecule such as acetonitrile where the formation of an extended hydrogen bonding network may not be possible.

Figure 9 displays the mass spectra obtained following the injection of $C_6H_6^{+\bullet}$ ions into the drift cell containing 0.20 Torr of acetonitrile vapor at two different temperatures. At 98 °C the major observed ions are $C_6H_6^{+\bullet}$ and $C_6H_6^{+\bullet}(CH_3CN)_n$ with $n = 1$ and 2. In addition small intensities corresponding to the clustering of one and two molecules of acetonitrile onto the $C_4H_4^{+\bullet}$ fragment ion of benzene are also observed. At −48 °C the $C_6H_6^{+\bullet}$ ion intensity decreases as the distribution shifts to higher acetonitrile clusters with the $C_6H_6^{+\bullet}(CH_3CN)_3$ now observed and the $C_6H_6^{+\bullet}(CH_3CN)_2$ cluster representing the most intense peak. In addition, small peaks corresponding to $C_6H_6^{+\bullet}(H_2O)(CH_3CN)_2$ and $H^+(H_2O)(CH_3CN)_3$ are also observed but the protonated acetonitrile clusters $H^+(CH_3CN)_n$ are not present. This may suggest that the deprotonation reaction could have occurred from the $C_6H_6^{+\bullet}(CH_3CN)_3$ cluster to produce $H^+(CH_3CN)_3$ which in the presence of water impurity forms rapidly the very stable cluster ion $H^+(H_2O)(CH_3CN)_3$. This cluster has been studied extensively and its unusual stability is attributed to the formation of a blocked structure consisting of a central hydronium ion (H_3O^+) solvated with three acetonitrile molecules through three $H_2O^+H\cdots NCCH_3$ relatively strong hydrogen bonds.[52] Alternatively, the deprotonation reaction could take place from the $C_6H_6^{+\bullet}(H_2O)(CH_3CN)_2$ cluster to produce $H^{+\bullet}(H_2O)(CH_3CN)_2$, which would immediately add a CH_3CN molecule to form the observed stable cluster $H^+(H_2O)(CH_3CN)_3$. The energetics of the deprotonation reactions in both the $C_6H_6^{+\bullet}(CH_3CN)_n$ and the $C_3H_3^+(CH_3CN)_n$ clusters will be discussed following the discussion of the binding energies of these systems.

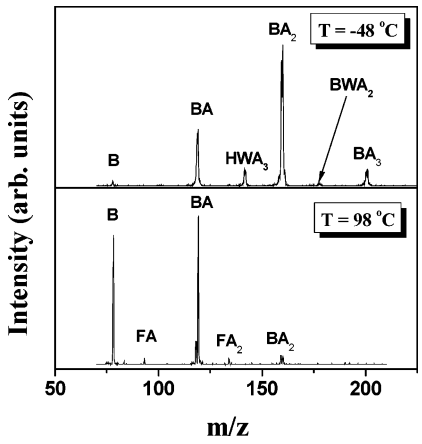

Figure 9. Mass spectra obtained following the injection of $C_6H_6^{+\bullet}$ ions (B, *m/z* 78) into 0.20 Torr of pure CH_3CN (A) vapor at different temperatures. W = H_2O, F = $C_4H_4^+$ fragment from the benzene cation.

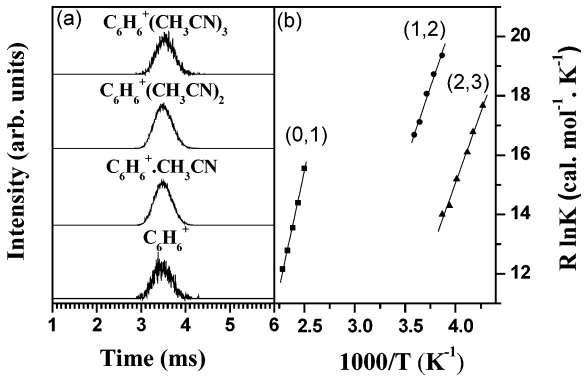

Figure 10. (a) Arrival time distributions (ATDs) of $C_6H_6^{+\bullet}(CH_3CN)_n$ clusters, $n = 0-3$, obtained by injecting $C_6H_6^{+\bullet}$ (*m/z* 78) into 0.17 Torr of pure CH_3CN vapor at 98 °C. (b) van't Hoff plots for the clustering equilibria: $C_6H_6^{+\bullet}(CH_3CN)_{n-1} + CH_3CN \rightarrow C_6H_6^{+\bullet}(CH_3CN)_n$ represented by $(n-1) - n$, with $n = 1-3$.

Figure 10a displays identical ATDs of $C_6H_6^{+\bullet}(CH_3CN)_n$ ions with $n = 0-3$, confirming that equilibrium has been established under the experimental conditions. The equilibrium constants for the stepwise solvation of $C_6H_6^{+\bullet}$ with 1−3 acetonitrile molecules yield the van't Hoff plots shown in Figure 10b. The resulting $\Delta H°$ and $\Delta S°$ values are listed in Table 3.

Figure 11 displays the mass spectra obtained following the injection of the $C_3H_3^{+\bullet}$ ions into the drift cell containing 0.1 Torr of acetonitrile vapor at different temperatures. As the

TABLE 3: Thermochemistry[a] of the Solvation Equilibria of $C_6H_6^{+\bullet}$ and $C_3H_3^+$ by Acetonitrile Molecules

n	$\Delta H°$ (kcal·mol^{-1})	$\Delta S°$ (cal·mol^{-1}·K^{-1})
	$C_6H_6^{+\bullet}(CH_3CN)_{n-1} + CH_3CN = C_6H_6^{+\bullet}(CH_3CN)_n$	
1	−15.1	−22.5
2	−10.5	−19.3
3	−9.4	−22.1
	$C_3H_3^+(CH_3CN)_{n-1} + CH_3CN = C_3H_3^+(CH_3CN)_n$	
1	−15.3	−21.5
2	−13.3	−18.2
3	−12.0	−21.6

[a] Error estimate for experimental values from standard deviations of van't Hoff and from usual uncertainties in clustering equilibrium temperature studies: $\Delta H° \pm 1$ kcal·mol^{-1}, $\Delta S° \pm 3$ cal·mol^{-1}·K^{-1}.

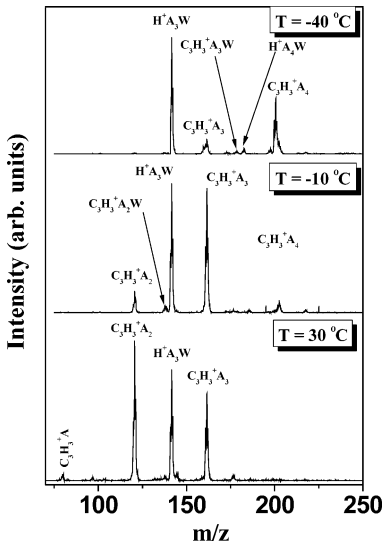

Figure 11. Mass spectra obtained following the injection of $C_3H_3^+$ ions (*m*/*z* 39) into 0.1 Torr of pure CH_3CN (A) vapor at different temperatures (W = H_2O).

temperature decreases, the distribution of the $C_3H_3^+(CH_3CN)_n$ cluster series shifts to larger *n*, and at −40 °C the $C_3H_3^+(CH_3CN)_4$ is the most populated ion among this series. Similar to the $C_6H_6^{+\bullet}/(CH_3CN)_n$ system, the $H^+(H_2O)(CH_3CN)_3$ cluster exhibits a remarkable enhanced population at all temperatures, again confirming the extra stability of this cluster. Figure 12a displays identical ATDs of $C_3H_3^+(CH_3CN)_n$ ions with $n = 1-3$, and Figure 12b shows the van't Hoff plots for the stepwise solvation of $C_3H_3^+$ with 1−3 acetonitrile molecules. The resulting $\Delta H°$ and $\Delta S°$ values are listed in Table 3.

Consistent with other hydrogen bonded systems, the results in Table 3 show that the highly polar acetonitrile molecules (μ = 3.6 D) bind to the $C_6H_6^{\bullet+}$ and $C_3H_3^+$ ions more strongly than water. For example, Table 3 shows that the first three CH_3CN molecules solvate $C_3H_3^+$ by 40.6 kcal/mol compared with 30.5 kcal/mol for three H_2O molecules (Table 1). In the case of solvation with CH_3CN molecules, the inner shell solvent molecules are attached by $CH^{\delta+}\cdots N$ type bonds to the core ion and the outer shell solvent molecules are attached similarly by $CH^{\delta+}\cdots N$ bonds to the methyl hydrogens of the inner shell molecules. Most bond strengths of this type are 8−10 kcal/mol, and therefore, starting an outer shell with CH_3CN molecules does not show a significant thermochemical effect. However, the effect of the smaller size and, consequently, the higher charge density of the $C_3H_3^+$ compared to the $C_6H_6^{\bullet+}$ ion is clearly demonstrated in the significantly higher binding energies of the second and third acetonitirle molecules to $C_3H_3^+$. This is a direct result of both charge−dipole and dipole−dipole

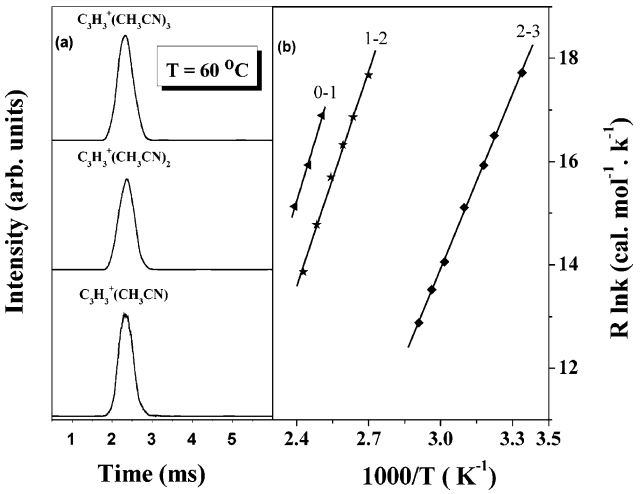

Figure 12. (a) Arrival time distributions (ATDs) of $C_3H_3^+(CH_3CN)_n$ clusters, $n = 1-3$, obtained by injecting $C_3H_3^+$ (*m*/*z* 39) into 0.1 Torr of pure CH_3CN vapor at 60°C. (b) van't Hoff plots for the clustering equilibria: $C_3H_3^+(CH_3CN)_{n-1} + CH_3CN \rightarrow C_3H_3^+(CH_3CN)_n$ represented by $(n-1) - n$, with $n = 1-3$.

interactions which exhibit strong distance dependences of $1/R^2$ and $1/R^3$, respectively.[53]

The stepwise deprotonation reaction in the $C_3H_3^+/(CH_3CN)_n$ cluster system is represented by

$$C_3H_3^+(CH_3CN)_{n-1} + CH_3CN \rightarrow (CH_3CN)_nH^+ + C_3H_2^{\bullet} \quad (8)$$

This reaction is endothermic by 26.1 kcal/mol for the $n = 2$ and 14.8 kcal/mol for the $n = 3$ step.[54] However, the corresponding reaction for $C_6H_6^{+\bullet}$ is exothermic for the $n = 3$ step because of the lower proton affinity of the $C_6H_5^{\bullet}$ radical (212 kca./mol) as compared to that of the $C_3H_2^{\bullet}$ radical (227 kcal/mol).[30] As a result, the deprotonation reaction could be observed in $C_6H_6^{+\bullet}(CH_3CN)_n$ clusters with $n = 3$. In both cases, $C_6H_6^{+\bullet}$ and $C_3H_3^+$, the mass spectra show significant abundance of the stable cluster ion $H^+(H_2O)(CH_3CN)_3$. This suggests that the presence of water facilitates the deprotonation reactions. In other words, the deprotonation reactions can become more exothermic by the incorporation of water molecules in the $C_6H_6^{+\bullet}(CH_3CN)_n$ and $C_3H_3^+(CH_3CN)_n$ clusters. In fact, the overall reaction $[M^+ + 3CH_3CN + H_2O \rightarrow H^+(H_2O)(CH_3CN)_3 + (M-H)^{\bullet}]$ is exothermic by 25.7 and 30.7 kcal/mol, for $M = C_3H_3^+$ and $C_6H_6^{+\bullet}$, respectively. The observations of the binary cluster ions $C_6H_6^{+\bullet}(H_2O)(CH_3CN)_2$ and $C_3H_3^+(H_2O)(CH_3CN)_2$ in the mass spectra support this suggestion. In this case, the generated $H^+(H_2O)(CH_3CN)_2$ ions within the neat acetonitrile vapor would immediately produce the terminated clusters $(H_3O^+)(CH_3CN)_3$ with methyl-blocked ligands that are not likely to add further acetonitrile molecules. It is interesting to note that the presence of a small water impurity can drive the deprotonation reactions in systems with blocked ligands that otherwise cannot form strong hydrogen bonded network that collectively removes the proton from the hydrocarbon ion.

IV. Summary, Conclusions and Outlook

We examined the gas-phase hydration, deprotonation and solvation of the $C_3H_3^+$ ion. Mobility and reactivity measurements indicate that we are observing the stable *c*-$C_3H_3^+$ isomer under our conditions. The binding energies of the hydrated clusters of about 9−12 kcal/mol and the somewhat stronger bonds to the more polar CH_3CN molecules are typical for

carbon-based $CH^+\cdots X$ hydrogen bonds. The measured binding energy and entropy change show unusual large values for the hydration of the *c*-$C_3H_3^+$ ion by four water molecules. Ab initio calculations show that the lowest energy isomers of the *c*-$C_3H_3^+$-$(H_2O)_3$ and *c*-$C_3H_3^+(H_2O)_4$ clusters consist of a cyclic water trimer and tetramer, respectively interacting with the *c*-$C_3H_3^+$ ion. For the *c*-$C_3H_3^+(H_2O)_4$ cluster, the cyclic water tetramer suggests the presence of orientational restraint of the water molecules consistent with the observed large entropy loss.

The thermochemistry for deprotonation becomes favorable by four or more H_2O molecules, due to the formation of strong hydrogen bonds in the product $(H_2O)_nH^+$ cluster ions. In case of solvation by blocked ligands such as acetonitrile molecules that cannot form extended hydrogen bonding network, the deprotonation reaction can be driven by the presence of mixed ligands that can form stable protonated clusters such as water/acetonitrile or methanol/acetonitrile. The observed behavior of the $C_3H_3^+$/water system is fully analogous to the benzene$^{+\bullet}$/water system, suggesting that similar phenomena may apply also in other reactions of ionized hydrocarbons with solvent molecules. We also observed analogous multibody associative charge transfer (ACT) reactions of benzene$^{+\bullet}$ and toluene$^{+\bullet}$ with olefins, where charge transfer is driven by the formation of covalent bonds in the product ions.[55−57]

In general, these associative transfer reactions are driven by the formation of strong bonds in the product ions. These associative proton or charge transfer reactions require the assembly of a multibody cluster, which is favored at low temperatures. Accordingly, these reactions show negative temperature coefficients, including unprecedented steep negative temperature dependence in the $C_3H_3^+$/water and benzene$^{+\bullet}$/water systems. The reactions may reach unit collision efficiency at sufficiently low temperatures. This can allow ionized polycyclic aromatics to affect polymerization and ion-induced formation of ices in low-temperature astrochemical environments.[58]

Acknowledgment. This work was supported by NASA (NNG04GH45G) and National Science Foundation (CHE-0414613) Grants. We thank Dr. Karl K. Irikura (NIST) for calculations on the proton affinities of C_3H_2 radicals.

References and Notes

(1) Hayhurst, A. N.; Jones, H. R. N. *Nature* **1982**, *296*, 61.
(2) Harris, S. J.; Weiner, A. M. *Annu. Rev. Phys. Chem*. **1985**, *36*, 31.
(3) Gerlich, D.; Horning, S. *Chem. Rev.* **1992**, *92*, 1509.
(4) Lopez, R.; del Rio, E.; Menendez, M. I.; Sordo, T. L. *J. Phys. Chem. A* **2002**, *106*, 4616.
(5) Liu, G.; Li, Z.; Ding, Y.; Fu, Q.; Huang, X.; Sun, C.; Tang, A. *J. Phys. Chem. A* **2002**, *106*, 10415−10422.
(6) Calcote, H. F.; Keil, D. G. *Pure Appl. Chem*. **1990**, *62*, 815.
(7) Hall-Roberts, V. J.; Hayhurst, A. N.; Knight, D. E.; Taylor, S. G. *Combust. Flame* **2000**, *120*, 578.
(8) Herbst, E.; Smith, D.; Adams, N. G.; McIntosh, B. J. *J. Chem. Soc., Faraday Trans*. 2 **1989**, 1655.
(9) Cernicharo, J.; Gottlieb, M.; Guelin, M.; Killian, T. C.; Paubert, G.; Taddeus, P.; Vritilek, J. M. *Astrophys. J.* **1991**, *368*, L39.
(10) Smith, D. *Chem. Rev.* **1992**, *92*, 1473.
(11) Wyss, M.; Riaplov, E.; Maier, J. P. *J. Chem. Phys.* **2001**, *114*, 10355.
(12) Moses, J. I.; Bezard, B.; Lellouch, E.; Gladstone, G. R.; Feuchtgruber, H.; Allen, M. *Icarus* **2002**, *143*, 244−298.
(13) Anicich, V. G.; Wilson, P.; McEwan, M. J. *J. Am. Soc. Mass Spectrom*. **2003**, *14*, 900.
(14) Lias, S. G.; Barmess, J. E.; Liebman, J. F.; Holms, J. L.; Levin, R. D.; Mallard, W. G. *J. Phys. Chem. Ref. Data* **1988**, *17* (Suppl 1).
(15) Scott, G. B. I.; Fairley, D. A.; Freeman, C. G.; McEwan, C. G.; Anicich, V. G. *J. Phys. Chem. A* **1999**, *103*, 1073.
(16) Scott, G. B. I.; Milligan, D. B.; Fairley, D. A.; Freeman, C. G.; McEwan, M. J. *J. Chem. Phys.* **2000**, *112*, 4959.
(17) Jeffrey, G. A.; Editor *An Introduction to Hydrogen Bonding*; Oxford University Press: Oxford, U.K., 1997.
(18) Sloan, E. D. *Clathrate Hydrates of Natural Gases*; M. Dekker: New York, 1990.
(19) Tanford, C. *The Hydrophobic Effect: Formation of Micelles and Biological Membranes*, 2nd ed.; Wiley: New York, 1980.
(20) Ibrahim, Y.; Alshraeh, E.; Dias, K.; Meot-Ner (Mautner), M.; El-Shall, M. S. *J. Am. Chem. Soc*. **2004,** *126*, 12766.
(21) Ibrahim, Y. M.; Meot-Ner (Mautner), M.; Alsharaeh, E. H.; El-Shall, M. S.; Scheiner, S. *J. Am. Chem. Soc*. **2005,** *127*, 7053.
(22) Meot-Ner (Mautner), M. *Chem. Rev.* **2005,** *105*, 213.
(23) Sieck, L. W.; Searles, S. K. *J. Chem. Phys.* **1970,** *53*, 2601.
(24) Daly, G. M.; Meot-Ner (Mautner), M.; Pithawalla, Y.; El-Shall, M. S. *J. Chem. Phys.* **1996,** *104*, 7965.
(25) Silverman, J.; Tagawa, S.; Kobayashi, H.; Katsumura, Y.; Washio, M.; Tabata, Y. *Radiat. Phys. Chem.* **1983**, *22*, 1039−1042.
(26) Mahmoud, H.; Germanenko, I. N.; Ibrahim, Y.; El-Shall, M. S. *J. Phys. Chem. A*, **2003,** *107*, 5920−5932.
(27) Mahmoud, H.; Germanenko, I. N.; Wright, D.; El-Shall, M. S. *J. Phys. Chem. A* **2005,** *109*, 4474−4483.
(28) Woon, D. E.; Park, J.-Y. *Astrophys. J.* **2004**, *607*, 342−345.
(29) Gudipati, M. S.; Allamandola, L. J. *Astrophys. J.* **2003**, *596*, L195-L198.
(30) Hunter, E. P.; Lias, S. G. Proton Affinity Evaluation. In *NIST Chemistry WebBook*; NIST Standard Reference Database Number 69; Linstrom, P. J., Mallard, W. G., Eds.; National Institute of Standards and Technology, Gaithersburg, MD, 20899, June 2005 (http://webbook.nist.gov).
(31) El-Shall, M. S.; Olafsdottir, S.; Meot-Ner, M.; Sieck, L. W. *Chem. Phys. Lett.* **1991**, *185*, 193.
(32) El-Shall, M. S.; Daly, G. M.; Gao, J.; Meot-Ner, M.; Sieck, L. W. *J. Phys. Chem*. **1992**, *96*, 507.
(33) Rusyniak, M. J.; Ibrahim, Y. M.; Wright, D. L.; Khanna, S. N.; El-Shall, M. S. *J. Am. Chem. Soc*. **2003**, *125*, 12001.
(34) Rusyniak, M.; Ibrahim, Y.; Alsharaeh, E.; Meot-Ner, M.; El-Shall, M. S. *J. Phys. Chem. A* **2003**, *107*, 7656.
(35) Ibrahim, Y.; Alsharaeh, E.; Rusyniak, M.; Watson, S.; Meot-Ner, M.; El-Shall, M. S. *Chem. Phys. Lett.* **2003**, *380*, 21.
(36) Frisch, M. J.; Trucks, G. W.; Schlegel, H. B.; Scuseria, G. E.; Robb, M. A.; Cheeseman, J. R.; Montgomery, J. A., Jr.; Vreven, T.; Kudin, K. N.; Burant, J. C.; Millam, J. M.; Iyengar, S. S.; Tomasi, J.; Barone, V.; Mennucci, B.; Cossi, M.; Scalmani, G.; Rega, N.; Petersson, G. A.; Nakatsuji, H.; Hada, M.; Ehara, M.; Toyota, K.; Fukuda, R.; Hasegawa, J.; Ishida, M.; Nakajima, T.; Honda, Y.; Kitao, O.; Nakai, H.; Klene, M.; Li, X.; Knox, J. E.; Hratchian, H. P.; Cross, J. B.; Adamo, C.; Jaramillo, J.; Gomperts, R.; Stratmann, R. E.; Yazyev, O.; Austin, A. J.; Cammi, R.; Pomelli, C.; Ochterski, J. W.; Ayala, P. Y.; Morokuma, K.; Voth, G. A.; Salvador, P.; Dannenberg, J. J.; Zakrzewski, V. G.; Dapprich, S.; Daniels, A. D.; Strain, M. C.; Farkas, O.; Malick, D. K.; Rabuck, A. D.; Raghavachari, K.; Foresman, J. B.; Ortiz, J. V.; Cui, Q.; Baboul, A. G.; Clifford, S.; Cioslowski, J.; Stefanov, B. B.; Liu, G.; Liashenko, A.; Piskorz, P.; Komaromi, I.; Martin, R. L.; Fox, J.; Keith, T.; Al-Laham, M. A.; Peng, C. Y.; Nanayakkara, A.; Challacombe, M.; Gill, P. M. W.; Johnson, B.; Chen, W.; Wong, M. W.; Gonzalez, C.; Pople, J. A. *Gaussian 03*, revision C.02; Gaussian, Inc.: Wallingford, CT, 2004.
(37) Rosenstock, H. M.; Dannacher, J.; Liebman, J. *Radiat. Phys. Chem*. **1982**, *20*, 7.
(38) Kuhlewind, H.; Kiermeier, A.; Neusser, H. J. J. *J. Chem. Phys.* **1986**, *85*, 4427.
(39) Van der Hart, W. J. *Inter. J. Mass Spectrom. Ion Processes* **1997**, *171*, 269.
(40) Mason, E. A.; McDaniel, E. W. *Transport Properties of Ions in Gases*; John Wiley & Sons: New York, 1988.
(41) Ellis, H. W.; McDaniel, E. W.; Albritton, D. L.; Viehland, L. A.; Lin, S. L.; Mason, E. A. Transport Properties of Gaseous Ions Over a Wide Energy Range. Part II. *At. Data Nucl. Data Tables* **1978**, *22*, 179−217.
(42) Liu, G.; Li, Z.; Ding, Y.; Fu, Q.; Huang, X.; Sun, C.; Tang, A. *J. Phys. Chem. A* **2002**, *106*, 10415−10422.
(43) Mesleh, M. F.; Hunter, J. M.; Shvartsburg, A. A.; Schatz, G. C.; Jarrold, M. F. *J. Phys. Chem.* **1996**, *100*, 16082.
(44) Smyth, K. C.; Lias, S. G.; Ausloos, P. *Combust. Sci. Technol*. **1982,** *28*, 147.
(45) Meot-Ner (Mautner), M.; Deakyne, C. A. *J. Am. Chem. Soc*. **1985,** *107*, 469.
(46) Deakyne, C. A.; Meot-Ner (Mautner), M. *J. Am. Chem. Soc*. **1985,** *107*, 474.
(47) Meot-Ner (Mautner), M.; Speller, C. V. *J. Phys. Chem.* **1986,** *90*, 6616.
(48) Meot-Ner (Mautner), M. In *Ion−Molecule Reactions*; Bowers, M. T., Ed.; Academic Press: New York, 1979; Vol. 1, pp 198−268.
(49) Ludwig, R. *Angew. Chem., Int. Ed. Engl*. **2001**, *40*, 1808−1827.
(50) Liu, K.; Cruzan; Saykally, R. J. *Science* **1996**, *271*, 929−933.
(51) Meot-Ner (Mautner), M.; Lias, S. G. Thermochemistry of Cluster Ions. In *NIST Chemistry WebBook*, NIST Standard Reference Database

Number 69; Linstrom, P. J., Mallard, W. G., Eds.; National Institute of Standards and Technology: Gaithersburg, MD, 20899, June 2005 (http://webbook.nist.gov).

(52) Deakyne, C. A.; Meot-Ner (Mautner), M.; Hughes, M. G.; Murphy, S. P. *J. Chem. Phys.* **1986**, *84*, 4598.

(53) Israelachvili, J. N. *Intermolecular and Surface Forces*, 2nd ed.; Academic Press: San Diego, 1992.

(54) Meot-Ner (Mautner), M. *J. Am. Chem. Soc.* **1978**, *100*, 4694.

(55) Meot-Ner (Mautner), M.; Pithawalla, Y.; Gao, J. L.; El-Shall, M. S. *J. Am. Chem. Soc.* **1997**, *119*, 8332.

(56) Pithawalla, Y.; M. S.; Mautner, M.; Gao, J. L.; El-Shall, M. S.; Baranov, V. I.; Bohme, D. K. *J. Phys. Chem. A.* **2001**, *105*, 3908.

(57) Ibrahim, Y.; Meot-Ner (Mautner), M.; El-Shall, M. S. *J. Phys. Chem. A*, submitted for publication.

(58) Allamandola, L. J.; Sandford, S. A.; Wopenka, B. *Science* **1987,** *237*, 56.